CHAPTER 4

The influence of interstitial carbon and nitrogen diffusion through the fusion line on the high temperature heat affected zone.

4.1. Introduction

It was suggested earlier that grain growth in the high temperature heat affected zone might be suppressed by increasing the levels of carbon and nitrogen in this region. Diffusion from the weld metal into the heat-affected zone was proposed as a method of increasing the interstitial levels locally. This chapter discusses the experimental procedure followed to test the approach and the results obtained.

The iron-chromium system can give rise to a wide variety of microstructures with markedly different mechanical properties. A particular characteristic of the iron-chromium equilibrium diagram (figure 4.1) is the restricted austenite phase field in the Fe-rich part of the diagram, most often called the gamma loop (γ -loop).

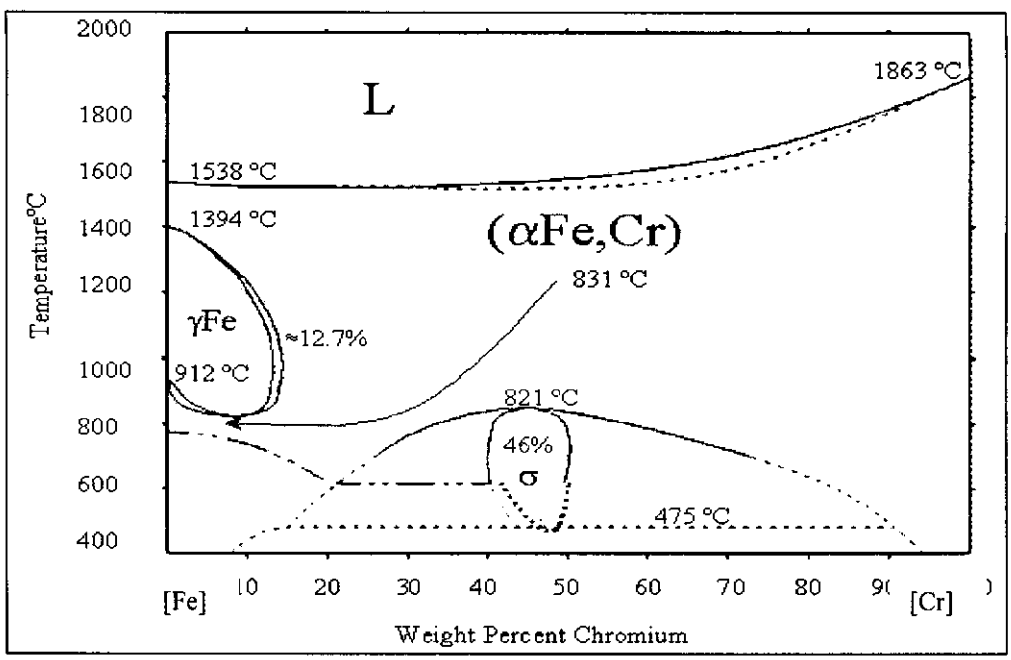

Figure 4.1: The iron-chromium equilibrium diagram.

The size of the gamma loop is essentially dependent on the relative amounts of austenite- and ferrite-formers in the steel. Elements like aluminum, vanadium, molybdenum, silicon and tungsten behave like chromium and promote the formation of delta ferrite[1]. Ferrite-formers tend to reduce the size of the gamma loop on the iron-chromium equilibrium diagram. On the other hand, elements like copper, manganese, cobalt, carbon and nitrogen behave like nickel and promote the formation of austenite[1]. Austenite-formers expand the gamma loop on the iron chromium diagram.

4.1.1 The influence of martensite

The room temperature microstructure of chromium steels can be predicted in part by considering two effects, namely[1]

1. The balance between austenite- and ferrite-formers, which dictates the microstructure at elevated temperatures.
2. The overall alloy content, which controls the M_s- and M_f- temperatures and the fraction retained austenite at ambient temperature.

A convenient method of relating composition and microstructure in stainless steel welds is by means of the Schaeffler diagram. This diagram is illustrated in figure 4.2. The Ni-equivalent equation used in the diagram indicates that carbon and nitrogen are approximately thirty times more effective in forming austenite than nickel. Although the Schaeffler diagram is only approximately correct for slow cooling rates, the fairly rapid cooling that takes place in a weld and its vicinity makes the diagram a useful tool in predicting the phase balance of stainless steel weld metals.

The Schaeffler diagram only provides information regarding the phase composition of the weld metal. The chemical composition of the heat-affected zone generally does not change during welding, and the region only determines the microstructure and phase composition by the thermal cycle experienced.

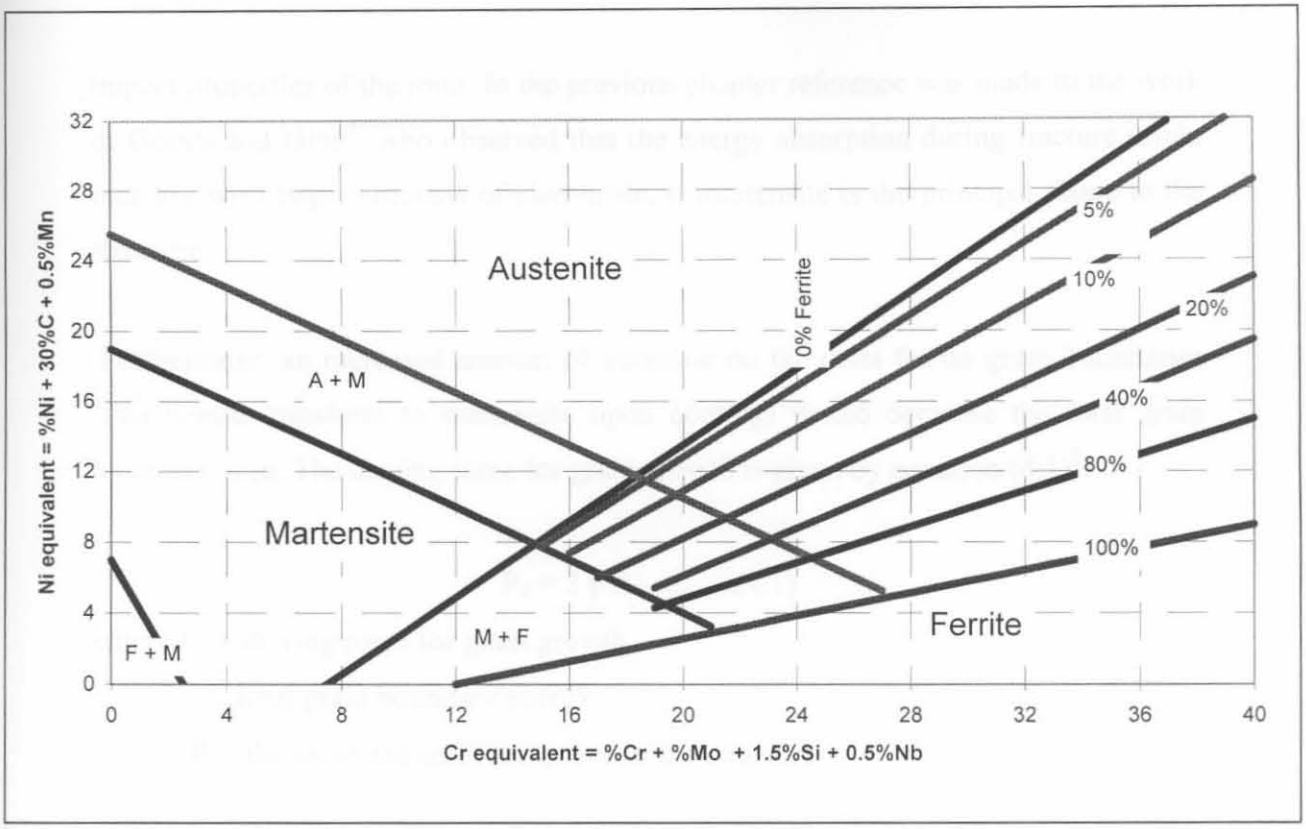

Figure 4.2: The Schaeffler diagram[2].

Ferrite grain growth takes place in the high temperature heat affected zone at temperatures above the austenite to delta ferrite transformation temperature, and leads to embrittlement of the zone. This may play a role in increasing the transition temperature [3,4,5].

Embrittlement may also occur in the weld metal, especially if a titanium or niobium stabilized filler metal is used[6]. The stabilizing precipitates decompose during welding, and re-precipitate in a finer form. Some of the titanium in the precipitate is replaced by chromium. As a result, residual titanium is present in the weld metal. The free titanium embrittles the weld metal, and has a negative effect on the impact properties of the joint[6]. However, this thesis is primarily concerned with embrittlement in the high temperature heat affected zone. In the heat-affected zone, ferrite grain growth is the major factor contributing to the embrittlement of the welded joint[1,3,4,5].

In the HTHAZ of 3CR12 welds, significant amounts of martensite are often present on the grain boundaries. The presence of martensite also has an influence on the

impact properties of the joint. In the previous chapter reference was made to the work of Gooch and Ginn[5], who observed that the energy absorption during fracture might increase with larger amounts of martensite, if martensite is the principal phase in the structure.

Furthermore, an increased amount of austenite on the delta ferrite grain boundaries (that would transform to martensite upon cooling) would decrease the total grain boundary area. The driving force for grain growth is given by equation (4.1)[7]:

$$P_d = 2\,\gamma/R \quad .....(4.1)$$

where P_d = driving force for grain growth

γ = total grain boundary energy

R = the mean radius of the grains in the structure

The γ -term, or the total grain boundary energy of the delta ferrite grains, would be reduced by the presence of a second phase (in this instance austenite) on the grain boundaries[7]. A second phase on the grain boundaries also acts as a physical obstacle to grain boundary movement, and the grain boundary must physically pull itself through the second phase inclusions in order for grain growth to take place[8].

The influence of large fractions of martensite in the heat-affected zone was studied during weld simulation experiments carried out by Zaayman[3]. The results were obtained by applying different thermal cycles to the same alloy. From the results (as shown in figure 4.3) it appears that increasing martensite levels are harmful to the impact properties of the structure up to a fraction of 90%, and that the DBTT decreases thereafter. The martensite on the grain boundaries induces high stresses in the softer adjacent ferrite. These stresses promote cleavage fracture[3]. An increase in the fraction martensite also decreases the effective grain size of the remaining ferrite. At higher fractions of martensite this effect dominates, and this accounts for the observed decrease in the DBTT[3].

4.1.2 The influence of carbon and nitrogen.

Carbon and nitrogen influence the impact properties of the heat-affected zone mainly in two opposing ways. In the first instance, the hardness of the intergranular martensite that forms in the high temperature heat affected zone increases with increasing carbon and/or nitrogen contents, which is detrimental to the impact properties[3]. Carbon and nitrogen are also strong austenite-formers, and can restrict delta ferrite grain growth by extending the dual phase austenite-ferrite structure to high temperatures[3]. The optimum amount of carbon and nitrogen is strongly dependent on the alloy content of the steel, and may therefore vary considerably. The combined effect of carbon and nitrogen on the size of the γ-loop is shown in figure 4.4. Although the microstructure of the heat affected zone in as-welded 3CR12 is not predominantly martensitic, an increase in the interstitial carbon and nitrogen contents of the heat affected zone could shift the %(C+ N) closer to the optimum indicated in figure 4.5.

In the case of a predominantly ferritic microstructure with a large ferrite grain size and grain boundary martensite, a higher carbon and nitrogen content may be detrimental to the impact properties of the joint. The martensite on the grain boundaries would be harder and more brittle with a higher interstitial content. If the structure contains a high fraction of martensite, the effect on the impact properties of the joint would be undesirable.

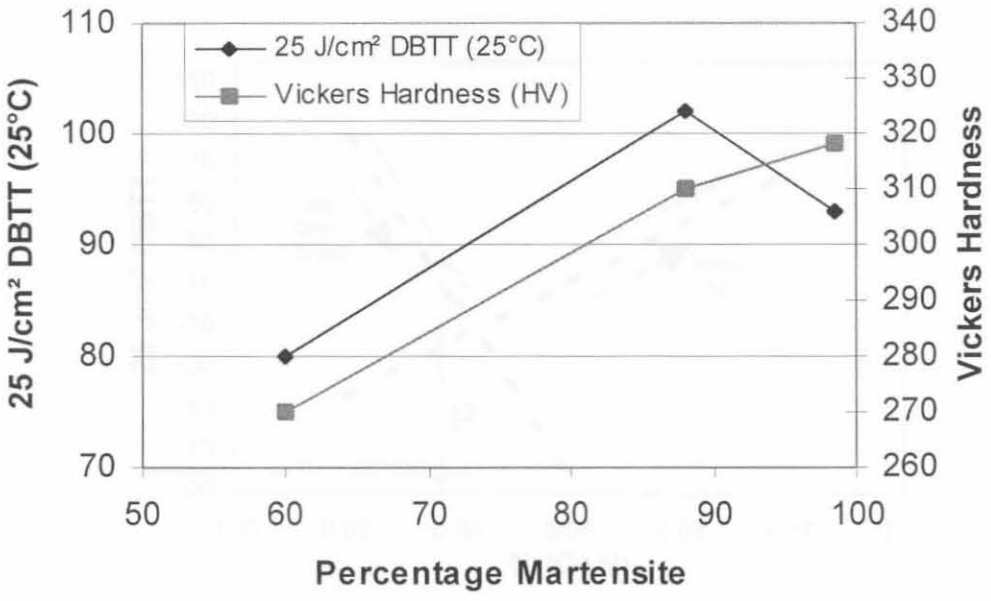

Figure 4.3: The influence of martensite content on the DBTT at a constant ferrite grain size[3].

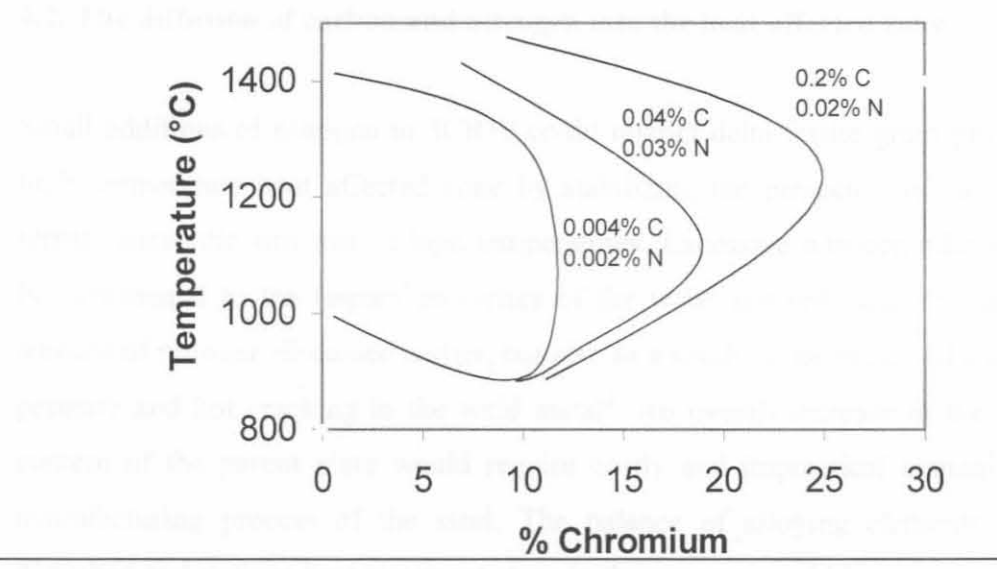

Figure 4.4: The influence of carbon and nitrogen on the size of the gamma loop on the Fe-Cr system[3].

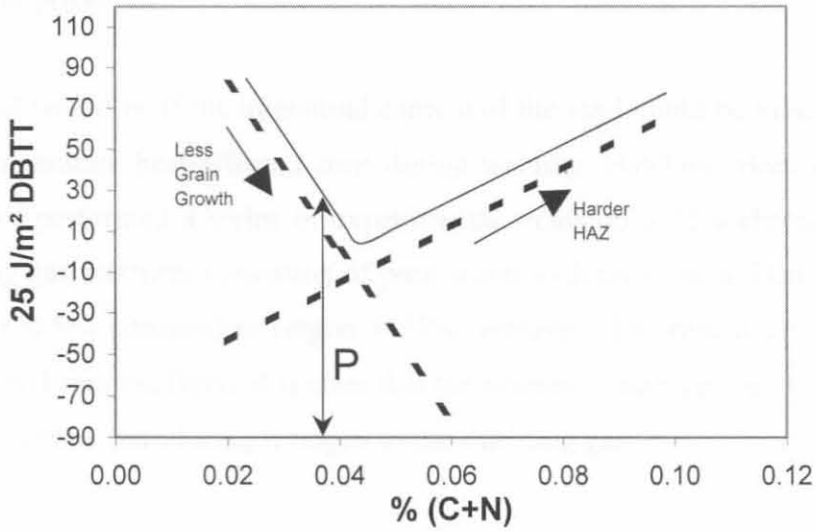

Figure 4.5: The influence of carbon and nitrogen on the DBTT of a predominantly martensitic structure[3].

4.2. The diffusion of carbon and nitrogen into the heat affected zone

Small additions of nitrogen to 3CR12 could restrict delta ferrite grain growth in the high temperature heat affected zone by stabilizing the prescence of a dual phase ferritic-austenitic structure at high temperatures. Excessive nitrogen additions would be detrimental to the impact properties of the weld, not only due to the optimum amount of nitrogen discussed earlier, but also as a result of the increased likelihood of porosity and hot cracking in the weld metal[2]. An overall increase in the interstitial content of the parent plate would require costly and impractical alterations in the manufacturing process of the steel. The balance of alloying elements would be disturbed and various heat treatment steps in the process would have to be altered. As one of the main advantages of 3CR12 is the relatively economical cost at which the steel can be made available to the consumer, an increase in the overall interstitial content, with subsequent alterations in the manufacturing process would not be practical. Increased carbon levels would necessitate an increase in chromium levels in

order to prevent sensitizing, which would inflate the raw material cost and the consumer price.

The ideal would be if the interstitial content of the steel could be raised locally in the high temperature heat-affected zone during welding. Hawkins, Beech and Valtierra-Gallardo[9] performed a series of experimental welds on a 12% chromium steel with shielding gas mixtures consisting of pure argon with nitrogen additions ranging from (argon + 0.5% nitrogen) to (argon + 75% nitrogen). The results are summarized in figure 4.6. From the figure it is clear that the amount of nitrogen in the weld metal can be increased by introducing nitrogen to the shielding gas.

In order to change the nitrogen content in the HTHAZ, nitrogen has to diffuse from the weld metal into the HAZ adjacent to the weld. If the fusion line is seen as a simple diffusion couple at a constant temperature, the concentration profile of nitrogen away from the fusion line into the parent metal can be represented by figure 4.7.

The concentration of nitrogen at a specific distance from the fusion line as represented by figure 4.7, is described by equation (4.2)[10], if interstitial diffusion into the heat affected zone is assumed to be equivalent to interstitial case hardening by diffusion, and geometrical effects are not taken into account. The geometrical shape of particles in a particle bed influences reaction rates to a great extent, but the geometrical effect can be neglected when the process is assumed to be similar to the case hardening of steel components in carbon or nitrogen rich atmospheres.

$$c = c_0 \operatorname{erfc} \{r/[2(Dt)^{1/2}\} \quad .....(4.2)$$

where c_0 = nominal concentration of nitrogen in the weld metal (the realtive solubilities in the liquid and the solid autenite should in reality be used)

c = concentration of nitrogen at a distance r from the fusion line

r = distance from the fusion line (cm)

D = diffusion coefficient for nitrogen in steel at the temperature at which diffusion takes place

t = time in seconds

$(Dt)^{1/2}$ = the diffusion distance as defined by Einstein (from Thelning[10])

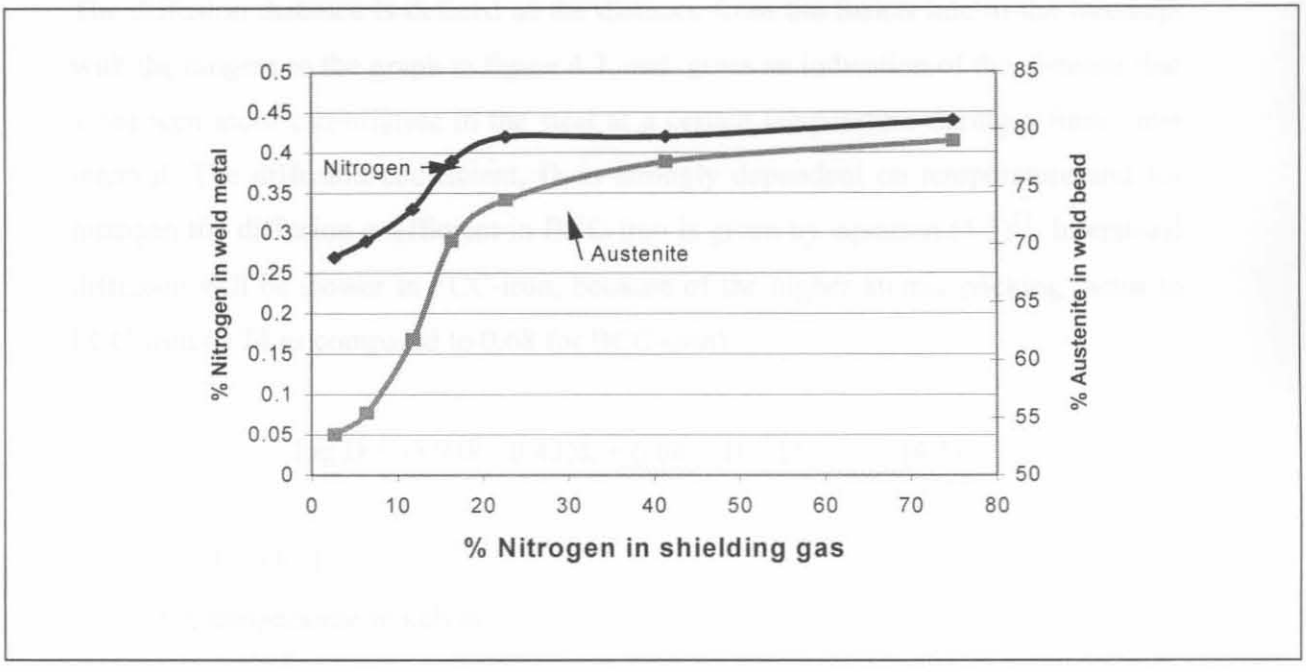

Figure 4.6: The nitrogen content of the weld metal as a function of the nitrogen content of the shielding gas during GMAW welding[9].

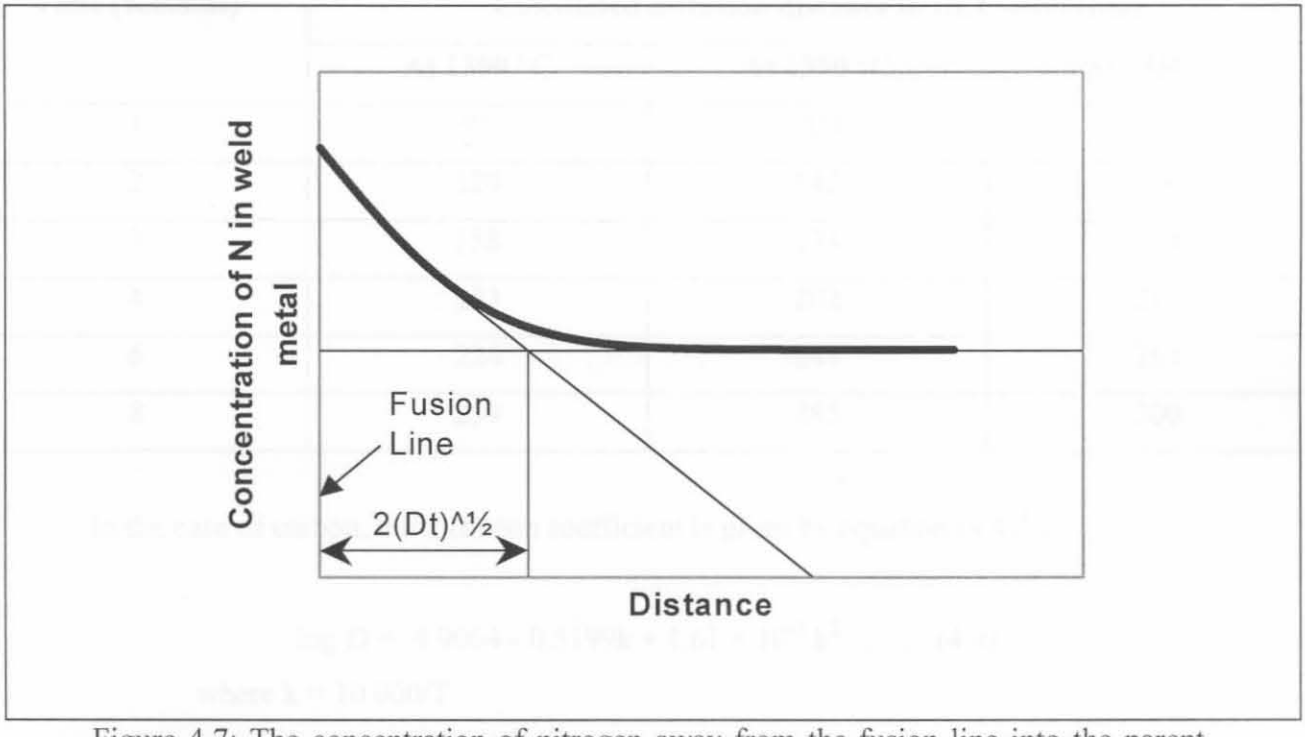

Figure 4.7: The concentration of nitrogen away from the fusion line into the parent metal after diffusion for time t at a constant temperature.

The diffusion distance is defined as the distance from the fusion line to the intercept with the tangent to the graph in figure 4.7, and gives an indication of the distance that a nitrogen atom can migrate in the steel at a certain temperature during a finite time interval. The diffusion coefficient, D, is strongly dependent on temperature and for nitrogen the diffusion coefficient in BCC-iron is given by equation (4.3)[11]. Interstitial diffusion will be slower in FCC-iron, because of the higher atomic packing factor in FCC-iron (0.74 as compared to 0.68 for BCC-iron)

$$\log D = -5.948 - 0.433k + 6.08 \times 10^{-4} k^2 \quad .....(4.3)$$

where $k = 10\,000/T$

T = temperature in kelvin

Using equations (4.2) and (4.3) the calculated diffusion distance was calculated for nitrogen at 1300 °C, 1350 °C and 1380 °C for intervals from 1s to 8s. The results are shown in table 4.1.

Table 4.1: Diffusion distances for nitrogen in BCC-iron at different temperatures.

Time (seconds)	**Calculated diffusion distance in BCC-iron (μm)**		
	At 1300 °C	**At 1350 °C**	**At 1380 °C**
1	91	100	106
2	129	142	150
3	158	174	184
4	183	202	213
6	224	247	261
8	259	285	300

In the case of carbon, the diffusion coefficient is given by equation (4.4)[11].

$$\log D = -4.9064 - 0.5199k + 1.61 \times 10^{-3} k^2 \quad .....(4.4)$$

where $k = 10\,000/T$

T = temperature in kelvin

The diffusion distance for carbon in BCC-iron was calculated in the same way as for nitrogen, and the results are shown in table 4.2.

Table 4.2: Diffusion distances for carbon in BCC-iron at different temperatures.

Time (seconds)	**Calculated diffusion distance in BCC-iron (μm)**		
	At 1300 °C	**At 1350 °C**	**At 1380 °C**
1	169	189	202
2	238	267	286
3	293	328	350
4	338	378	404
6	414	463	495
8	478	535	571

Isothermal conditions are implicitly assumed in the above calculations. This assumption is not valid, as the welded plate is cooling continuously. The temperature cycle experienced by a point at any distance away from the center line of a weld can be predicted using the Rosenthal equation. The Rosenthal equation assumes heat flow from a point source, which implies that the temperature at this point (at the weld centre line) reaches infinity. The equation also assumes that the material properties (thermal capacity, diffusivity, conductivity) do not change with temperature and it neglects heat losses at the plate surface, as well as the latent heat change due to any phase transformations that may occur. In spite of these limitations, the temperature field in the heat-affected zone is well represented by the Rosenthal equation[2]. In most practical welding situations, the velocity of the arc along the workpiece is much higher than the thermal diffusion rate. In other words, heat flow in the direction of travel is small compared to that perpendicular to the travel direction[2]. Furthermore, for a given weld geometry, material and process, the cooling time through the range 800 °C to 500 °C is constant in the heat affected parent plate.

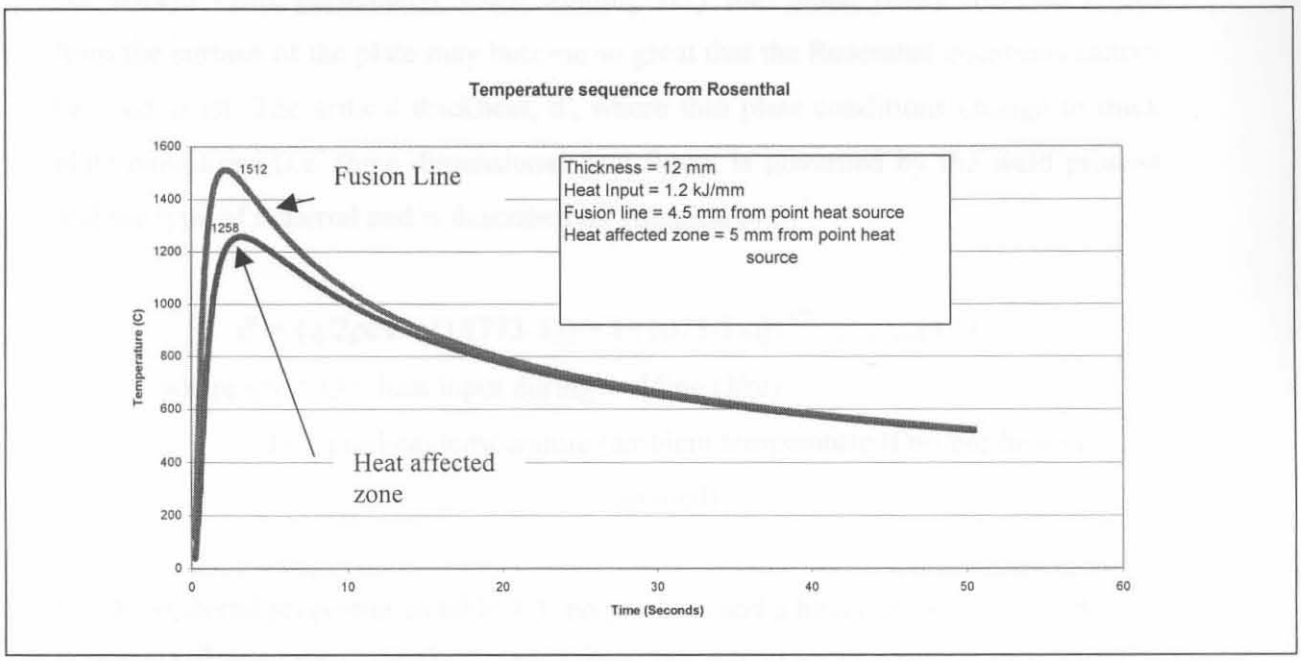

Figure 4.8: The welding temperature sequence as predicted from the Rosenthal equation[2].

On the basis of these assumptions, Rosenthal[2] determined the solutions to the heat flow equations of a moving point heat source in 1935[2]. Good evidence exists that the Rosenthal equations have agreeable validity in describing the temperature distribution about a weld[2]. In order to solve the equation, certain thermal and material properties of the parent plate are required in the Rosenthal equation. Various sources[2,12,13,14] were used to obtain these properties for the 3CR12 parent plate. The properties are tabulated in table 4.3.

Table 4.3: Thermal and material properties for 3CR12.

Melting Point	**Specific Gravity (ρ)**	**Specific Heat (C)**	**Thermal Conductivity (λ)**	ρC
1773 K	7700 kg/m^3	510 J/kgK	26 J/msK	3.93×10^6 J/m^{3}K

Rosenthal derived two different equations for thick and thin plate conditions. In the thin plate equation heat flow is considered to be two-dimensional. This assumption is

not always valid, particularly when welding very thin plate, where the heat losses from the surface of the plate may become so great that the Rosenthal equations cannot be used at all. The critical thickness, d', where thin plate conditions change to thick plate conditions (i.e. three dimensional heat flow), is governed by the weld process and the type of material and is described by equation (4.5)[2].

$$d' = \{q/2\rho cv \times [1/(773-T_0) + 1/(1073-T_0)]\}^{1/2} \quad .....(4.5)$$

where $q/v = Q$ = heat input during welding (J/m)

T_0 = pre-heat temperature (ambient temperature if no pre-heat is applied)

For the material properties in table 4.3, no pre-heat and a heat input during welding of $Q = 1 \times 10^6$ J/m, d' equals 21mm. Therefore, the thin plate equation must be used to predict the temperature cycle in a 12 mm 3CR12 plate. The Rosenthal equations for thin plate conditions are given by equations (4.6) through (4.9).

$$T_p - T_0 = (2/\pi e)^{1/2} \times Q/(d\rho c2r) \quad .....(4.6)$$

$$\Delta t = Q^2/(4\pi\lambda\rho c\Theta_2^2 d^2) \quad .....(4.7)$$

$$1/\Theta_2^2 = 1/(773-T_0)^2 - 1/(1073-T_0)^2 \quad .....(4.8)$$

$$T-T_0 = \Theta_2 \times (\Delta t/t)^{1/2} \times \exp\{-[\Theta_2^2 \Delta t]/[2et(T_p - T_0)^2]\} \quad .....(4.9)$$

where d = plate thickness

r = distance from the point-heat source perpendicular to the welding direction

e = the base of natural logarithms ($e \approx 2.718$)

T_p = peak temperature reached at distance r

The other variables are defined in table 4.3.

Assuming that the fusion line represents a peak temperature equal to the liquidus temperature of 3CR12, calculation yields the distance from the point source to the fusion line (T_p = 1773K) of a 1.0 kJ/mm weld on a 12mm 3CR12 plate to be 3.6mm.

The mean distance from the fusion line to the end of the grain growth zone is 200μm (ten measurements, 0.95 confidence level = 1.7μm). As a result, the end of the grain growth zone would be 3.8mm from the point source. If another 200μm is added for the remainder of the heat affected zone, the edge of the heat affected zone would be approximately 4mm from the point source. The measured value of 4.5mm from the center to the fusion line used in figure 4.8 was determined from a heat input of 1.2 kJ/mm, while welds used for this calculations were made at 1.0 kJ/mm. Through substitution and calculation, equation (4.9) can be written as

$$T\text{-}T_0 = 2328/t^{1/2} \times \exp[-(0.46/t)] \quad \text{.....(4.10)}$$

for the fusion line (3.6mm from the point source)

$$T\text{-}T_0 = 2328/t^{1/2} \times \exp[-(0.55/t)] \quad \text{.....(4.11)}$$

for the edge of the HTHAZ (3.8mm from the point source)

$$T\text{-}T_0 = 2328/t^{1/2} \times \exp[-(0.60/t)] \quad \text{.....(4.12)}$$

for the edge of the HAZ (4.0 mm from the point source)

The temperature cycles during the welding of 3CR12 plate can be calculated using equations (4.10) to (4.12). The area between fusion line and the edge of the coarse grain heat affected zone can be viewed as a series of successive peak temperatures to which the coarse delta ferrite structure is heated during welding.

It has already been stated that the nitrogen content of the weld metal can be increased effectively by adding nitrogen gas to a pure argon shielding gas[7]. The carbon content of the weld metal may be increased by welding with a filler metal containing a higher carbon content, such as E307.

The Rosenthal prediction (as shown in figure 4.8) states that the fusion line of a weld produced with a heat input of 1.2 kJ/mm in a 12 mm plate would be above 1400 °C for approximately 3 seconds. At a temperature of 1380 °C carbon can diffuse 202μm in 1 second and nitrogen can diffuse 106μm in the same time interval (see tables 4.1 and 4.2). This indicates that nitrogen can diffuse at least 106μm and carbon 202μm

away from the fusion line if the temperature were 1380°C or higher for 1 second in a weld performed with the same welding parameters.

The predicted diffusion data implies that it is possible to increase the interstitial content of the high temperature heat affected zone during welding by diffusion from the weld metal, as the measured width of the high temperature zone is in the proximity of 200μm. The width of the grain growth zone is typically a function of the heat input, but for the welding parameters used for the Rosenthal prediction, diffusion appears to be a practical method of increasing the interstitial content locally in the high temperature heat affected zone.

An increase in the interstitial content of the heat-affected zone would cause the gamma loop on the iron-chromium equilibrium diagram to expand. This will guarantee the existence of a larger amount of austenite on the delta ferrite grain boundaries at elevated temperatures during welding. The resulting decrease in total grain boundary energy would reduce the driving force for grain growth[7], and would inhibit the delta ferrite grain growth that occurs in the high temperature heat affected zone.

4.3 Experimental welds and results

In order to evaluate the effectiveness of the above-mentioned approach, a series of welds were produced using pure argon and argon-nitrogen shielding gas mixtures, or a high carbon filler metal. The microstructure and the toughness of the resulting welds were investigated.

4.3.1 Gas metal arc welding with E309L

The first series of welds were produced as a reference using the gas-metal-arc-welding process (GMAW) on a 12mm 3CR12 plate. Pure argon shielding gas and a 1.2mm diameter 309L filler wire were used. The heat input was maintained at 1.2 kJ/mm and a K-type weld preparation was utilized. The microstructures obtained in

the high temperature heat affected zone of the welds are typical of the microstructures discussed in the previous chapter, consisting of large delta ferrite grains with blocky martensite on the grain boundaries. A typical microstructure is shown in figure 4.9

The grain size in the high temperature heat affected zone was measured using two different methods. In the first place, a line intercept method was used. Four different counts of grain boundaries intercepting a line of constant length were made. Equation (4.13) (Hillards-equation) was used to determine the ASTM grain size number in the heat affected zone.

$$N = -10.0 - 6.64\log [L/(nM)] \quad .....(4.13)$$

where L = length of line (cm)

n = amount of grain boundaries intercepting the line (the grain size was taken as the size of the ferrite + the martensite)

M = magnification

N = ASTM grain size number

Standard ASTM eyepieces were also used to determine the range of the grain size. The corresponding grain size in microns was also obtained from data in the ASTM standards, part 1-A, 1946. In the ASTM method, $n = 2^{N-1}$, where n equals the number of grains per square inch at a magnification of 100×. Consequently, the greater the value of N, the smaller the average diameter of the grains.

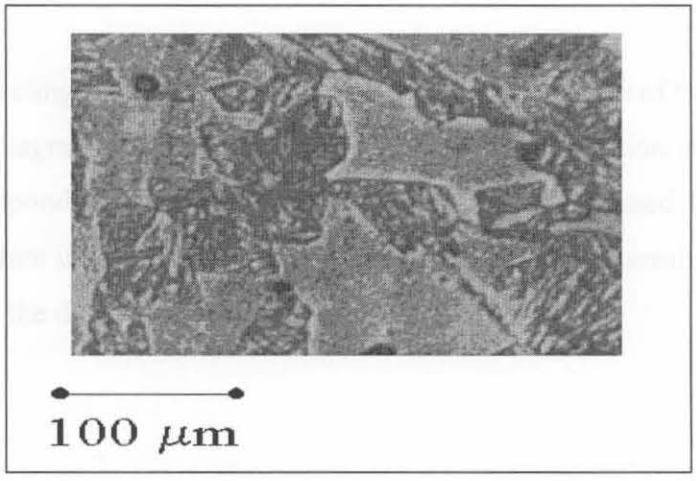

Figure 4.9: The high temperature heat affected zone. (GMAW, HI = 1.2 kJ/mm, 309L filler wire pure Argon shielding gas).

The ferrite number (which represents the magnetic response of the sample) of the weld metal was measured using a Fischer Feritscope™. The relationship between the ferrite number and the percentage ferrite is shown in figure 4.10. Ferrite number measurements are inherently more accurate than point counting. For this reason, the Feritscope was used to quantify the amount of ferrite in the weld metal. The average ferrite number obtained from ten different readings on each sample was 15.1FN. Using Kalling's no. 2 to etch the samples, the ferrite is observed as a light coloured phase. Using figure 4.10, a ferrite percentage corresponding to a ferrite number of 15.1 could be determined. The weld metal was found to contain approximately 13.4% ferrite.

Table 4.4: ASTM grain size numbers in the high temperature heat affected zone (GMAW, 1.3kJ/mm, E309L filler wire, pure argon shielding gas)

Number	**L (cm)**	**n**	**M**	**N**	**N from ASTM eyepiece**	**Matching grain size (μm)**
1	25.1	5	400	2.6	1-2	200-300
2	25.1	5	400	2.6	1-2	200-300
3	25.1	4	400	1.9	1-2	200-300
4	25.1	4	400	1.9	1-2	200-300
Average				2.25		

A tie line connecting the parent metal position and the position of the filler metal on the Schaeffler diagram was used to estimate the amount of dilution in the weld metal. The line corresponding to the parent metal and filler metal used is shown on the Schaeffler diagram in figure 4.11. If 13.4% ferrite is used to determine the position of the weld metal, the dilution is estimated at 45%.

4.3.2 Charpy V-notch values at 20 °C

Fifteen Charpy specimens were machined from the welded plate. As mentioned earlier, a K-type weld preparation with a pre-welded layer on the flat side was used (see figure 3.3). Precise placement of the Charpy notch into the high temperature heat affected zone was still difficult, and weld metal, parent metal and heat affected zone failures occurred. The heat affected zone failures appeared bright and uneven. The parent metal fractures were ductile with considerable plastic deformation around the edges of the specimen. The weld metal failures were dull fractures with no or very little plastic deformation. The results of the impact tests are shown in figure 4.12. All the fractures obtained could be divided into either the HAZ, parent metal or weld metal failures, and it appears that if a crack initiated in the coarse grained heat affected zone, it would travel straight through the zone without swerving into the parent metal or the weld metal, and this resulted in very low impact energies being recorded for the heat affected zone failures. The conclusion can be drawn that the butter layer method is effective if the notch can be directed accurately into the heat affected zone, and that the true impact properties of the heat affected zone can be measured. The results also indicate that the impact properties of the heat affected zone are inferior to those of the weld and parent metal, but it has to be emphasized once again that the butter layer K-type preparation can be described as a worst case situation, and that intergranular heat affected zone failures rarely occur in practice[1]. It is important to realize that stress raisers in the coarse grained region should be avoided in practice, and that brittle fracture may occur if proper design and preparation procedures are not followed.

4.3.3 Shielded metal arc welding with E309L and E307

A high carbon austenitic shielded metal arc welding electrode is also commercially available in the market, and the use of these electrodes was investigated. The second series of welds were produced using shielded metal arc welding and 8mm 3CR12 plate. The heat input was maintained at 0.7kJ/mm. In order to investigate the influence of a higher carbon filler on the HTHAZ properties, two electrode were used,

containing 0.03% (E309L) carbon and 0.16% carbon (E307) respectively. The microstructure in the high temperature heat affected zone of the E307 weld, as shown in figure 4.13 contains higher fractions of martensite on the grain boundaries, while the grain size of the remaining ferrite is smaller than in the E309L weld. The microstructures in the weld metal of both welds consisted of austenite and ferrite, and the ferrite numbers obtained from Fischer Ferritscope readings were 15.5FN for the E309L electrode and 13.1FN for the E307 electrode respectively.

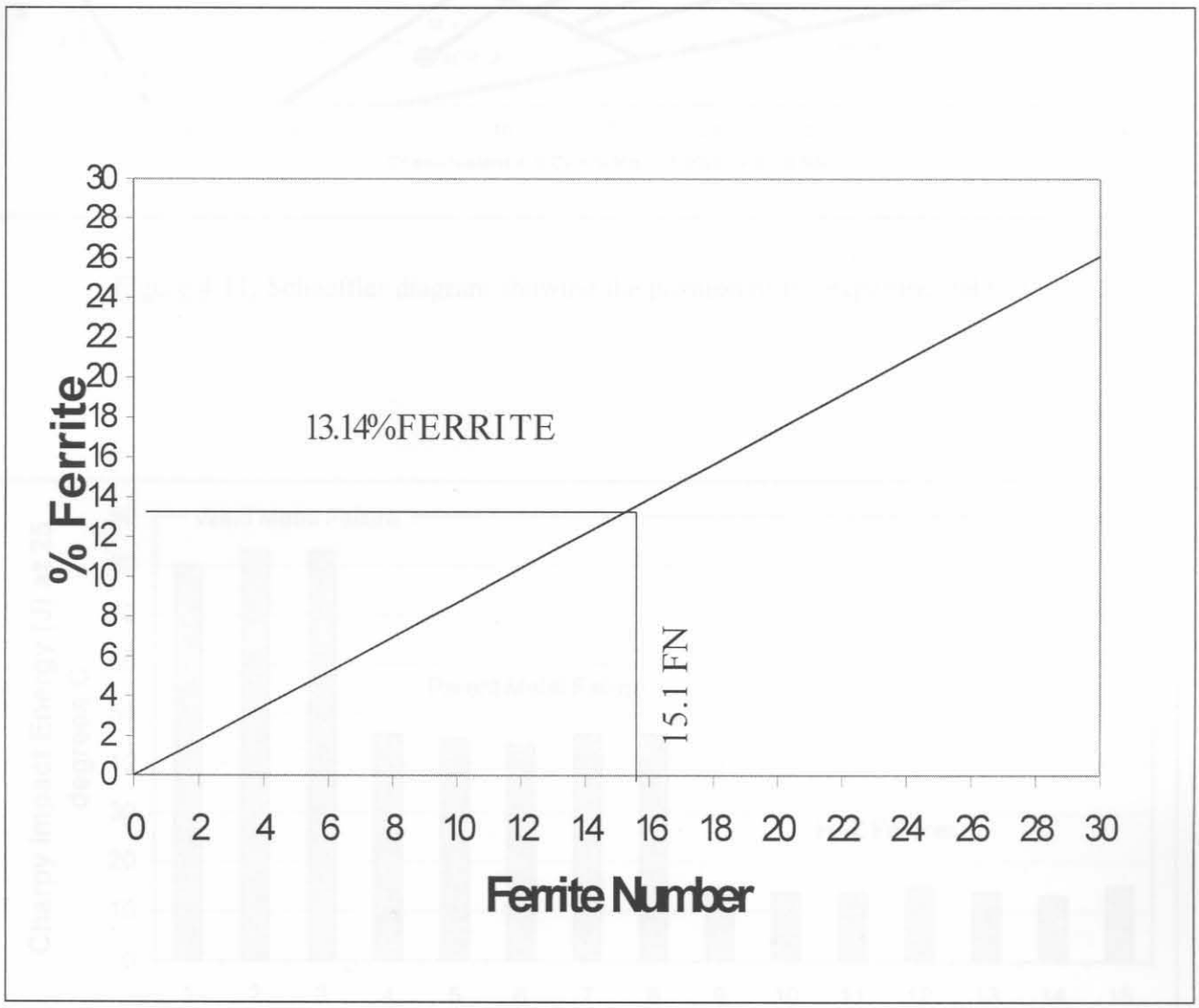

Figure 4.10: The relationship between ferrite number and percentage ferrite. (After the DeLong diagram, by William T. DeLong, revised January 1973)

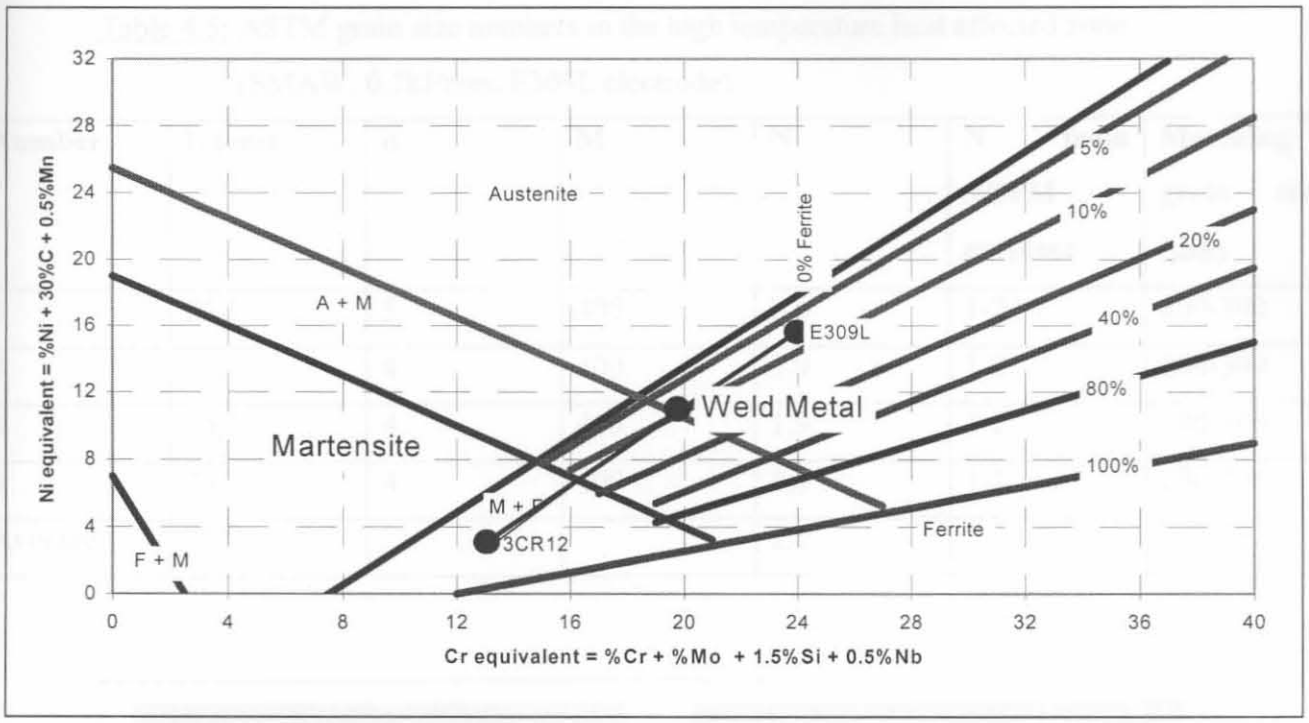

Figure 4.11: Schaeffler diagram showing the position of the experimental weld

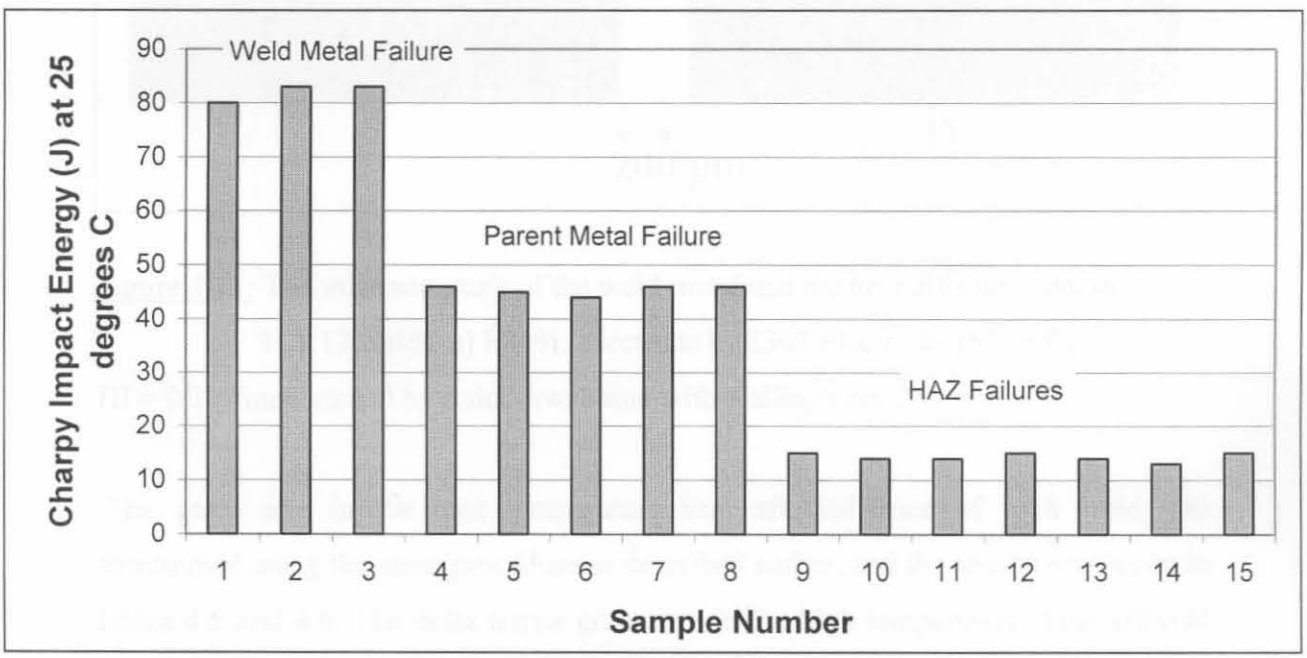

Figure 4.12: Charpy Impact Energy values at 25°C (GMAW, HI = 1.3kJ/mm, E309L filler wire, pure argon shielding gas)

Table 4.5: ASTM grain size numbers in the high temperature heat affected zone (SMAW, 0.7kJ/mm, E309L electrode)

Number	L (cm)	n	M	N	N from ASTM eyepiece	Matching grain size (μm)
1	25.1	5	400	2.6	1-2	200-300
2	25.1	4	400	1.9	1-2	200-300
3	25.1	4	400	1.9	1-2	200-300
4	25.1	4	400	1.9	1-2	200-300
Average				2.1		

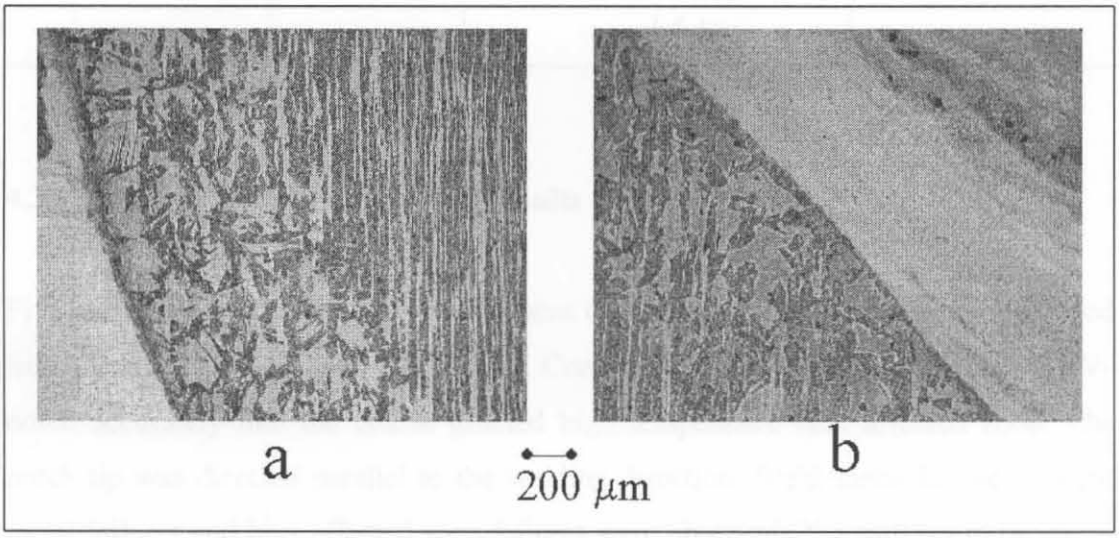

Figure 4.13: The microstructure of the weld metal and the heat affected zone in 3CR12 welds. a) E309L Electrode b) E307 Electrode. (SMAW, HI = 0.7kJ/mm, etched by quick swabbing with Kalling's no. 2)

The grain size in the high temperature heat affected zone of each weld was determined using the same procedure as described earlier, and the results are shown in tables 4.5 and 4.6. The delta ferrite grain size in the high temperature heat affected zone of E307 welds is smaller than the grain size obtained in the coarse grained zone of E309L welds. Furthermore, a larger fraction of martensite is present on the ferrite grain boundaries of E307 welds. Image analysis readings yielded 43% martensite on the delta ferrite grain boundaries in the high temperature heat affected zone of the

E307 welds, and 34% grain boundary martensite in the corresponding zone of the E309L welds.

Table 4.6: ASTM grain size numbers in the high temperature heat affected zone (SMAW, 0.7kJ/mm, E307 Electrode)

Number	**n**	**L (cm)**	**M**	**N**	**N from ASTM Eyepiece**	**Matching grain size (μm)**
1	25.1	13	400	5.4	4-5	70-80
2	25.1	12	400	5.1	4-5	70-80
3	25.1	11	400	4.9	4-5	70-80
4	25.1	11	400	4.9	4-5	70-80
Average				5.1		

4.3.3.1 Charpy V-notch testing and results

Five half size Charpy impact test specimens (10mm × 5mm × 55mm) were machined from each of the E309L and E307 welds. Considerable care was taken to direct the V-notch accurately into the coarse grained high temperature heat affected zone. The notch tip was directed parallel to the welding direction. Weld metal failures, parent metal failures and heat affected zone failures were observed. The failures in the grain growth zone of the E309L welds were bright and shiny intergranular fractures, and the crack propagated through the heat affected zone without deviating into the parent metal or the weld metal. The heat affected zone failures in the E307 welds showed deviation into the parent metal in the center of the fracture surface, and the crack appeared to swerve away from the harder heat affected zone into the parent metal, resulting in higher absorbed Charpy impact energy values. Hardness profiles across the two different welds are shown in figure 4.14 and the Charpy impact energy results are shown graphically in figure 4.15. It is evident that, although the E307 weld metal is harder than the E309L, it is still lower than the hardness of the heat affected zone. This suggested that protection of the HAZ by plastic deformation of the weld metal could as a result also occur when E307L is used as filler. The HAZ of the E307

welds has higher Charpy impact energy values, and may be more likely to be protected by plastic deformation of the weld metal and the 3CR12 parent metal.

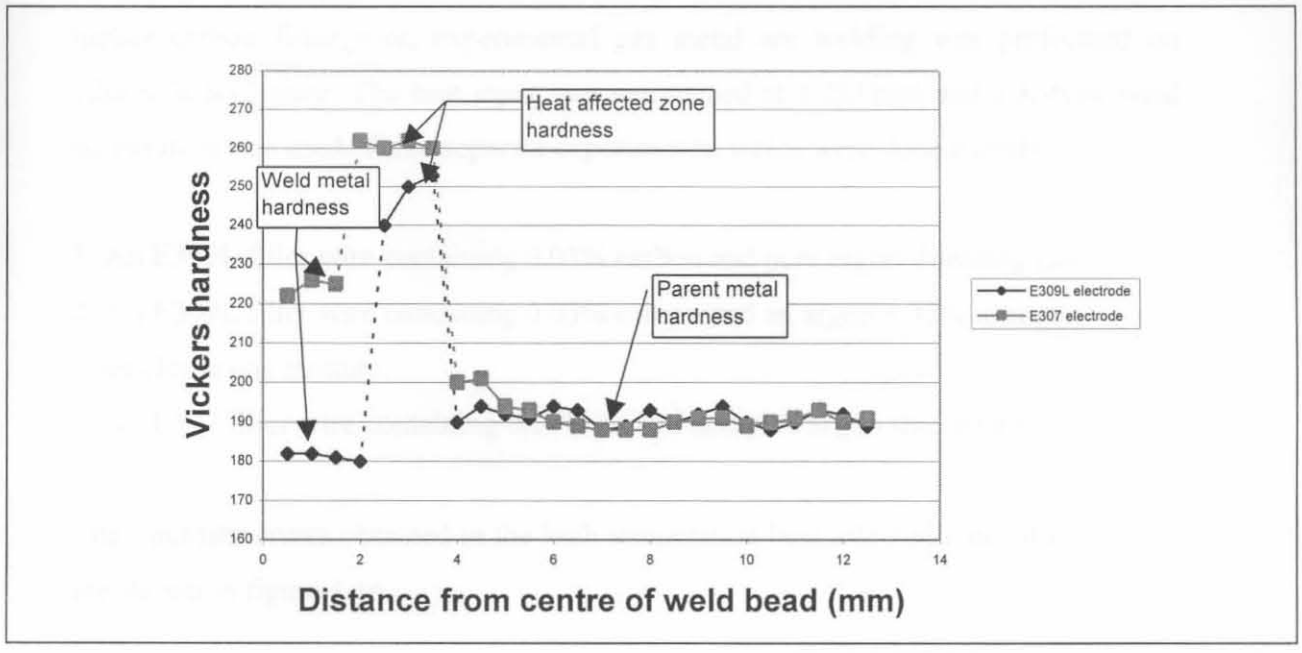

Figure 4.14: Hardness profile for welds in 3CR12 (SMAW, HI = 0.7kJ/mm)

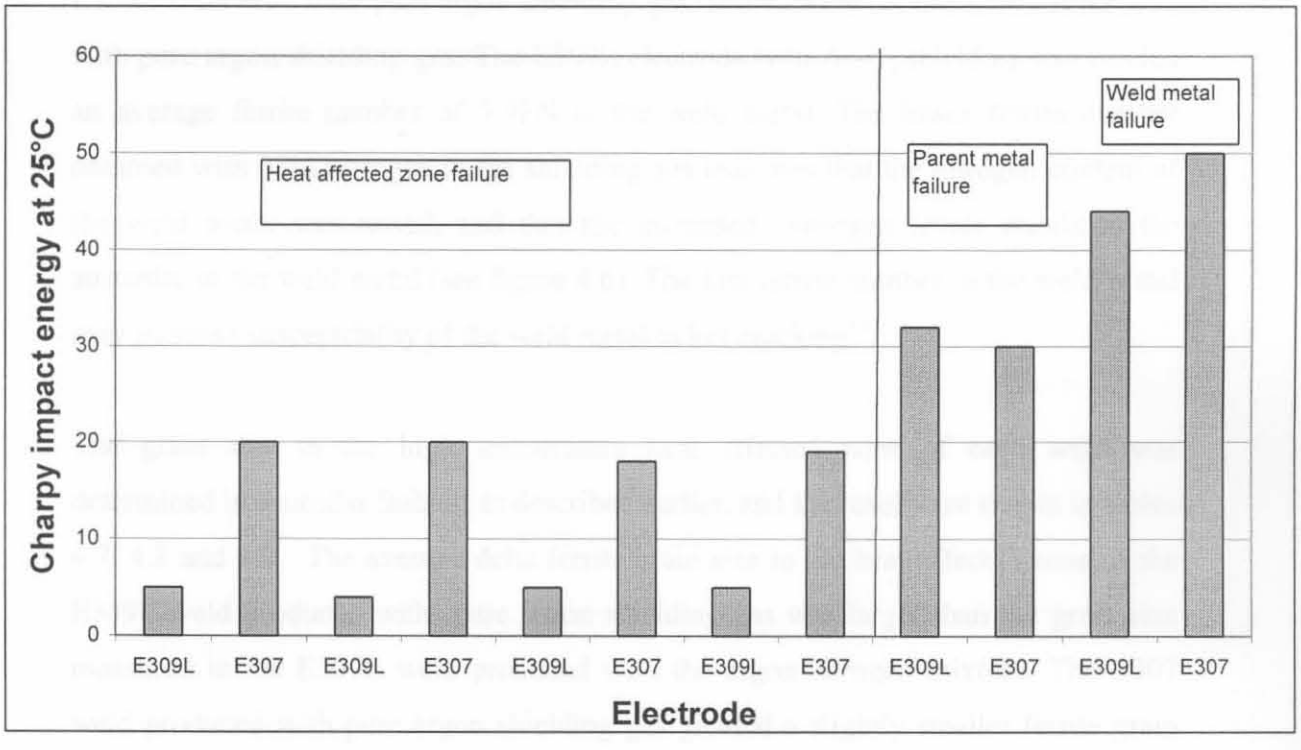

Figure 4.15: Charpy Impact Energy values at 20 °C (SMAW, HI = 0.7kJ/mm)

4.3.4 Gas metal arc welding with E309L (Ar and Ar+N_2) and E307 (Ar)

In order to investigate the influence of nitrogen additions to the shielding gas, and a higher carbon filler wire, experimental gas metal arc welding was performed on 12mm 3CR12 plate. The heat input was maintained at 1.2kJ/mm and a K-type weld preparation was used. Three separate experimental welds were done namely:

1. An E309L filler wire containing 0.03% carbon and pure argon shielding gas.
2. An E309L filler wire containing 0.03% carbon and an argon + 33% nitrogen shielding gas mixture.
3. An E307 filler wire containing 0.16% carbon and pure argon shielding gas.

The microstructures obtained in the high temperature heat affected zone of each weld are shown in figure 4.16.

The microstructure in the weld metal of each weld consisted of austenite and ferrite. The average ferrite numbers from Fischer Ferritscope readings were 15.1FN for the E309L filler wire with pure argon shielding gas, and 12.8FN for the E 307 filler wire with pure argon shielding gas. The E309L electrode with Ar-N_2 shielding gas yielded an average ferrite number of 5.9FN in the weld metal. The lower ferrite number obtained with 33% nitrogen in the shielding gas indicates that the nitrogen content of the weld metal was raised, and that the increased nitrogen levels stabilized the austenite in the weld metal (see figure 4.6). The low ferrite number in the weld metal may increase susceptibility of the weld metal to hot cracking[12].

The grain size in the high temperature heat affected zone of each weld was determined in a similar fashion as described earlier, and the results are shown in tables 4.7, 4.8 and 4.9. The average delta ferrite grain size in the heat affected zone of the E309L weld produced with pure argon shielding gas was larger than the grain size measured in the E309L weld produced with the argon-nitrogen mixture. The E307 weld produced with pure argon shielding gas yielded a slightly smaller ferrite grain size in the high temperature heat affected zone compared to the E309L welds.

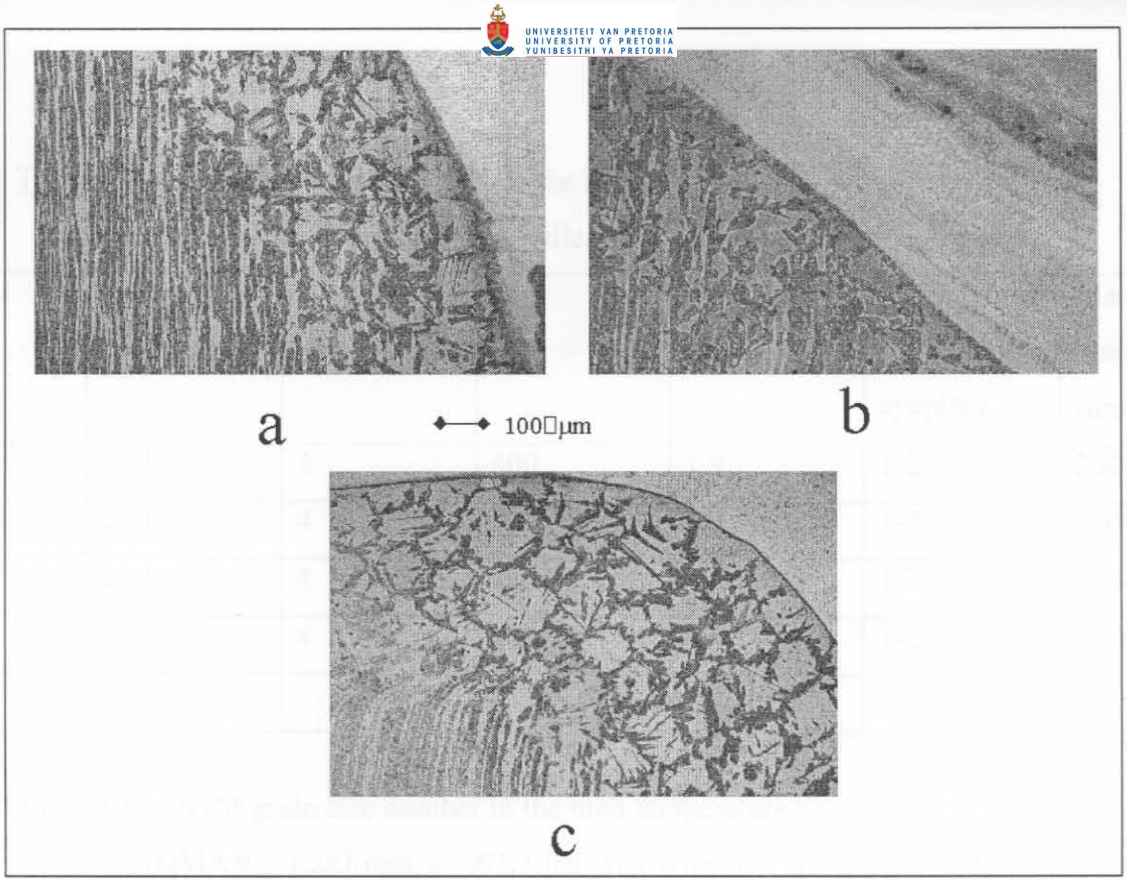

Figure 4.16: The microstructure of the weld metal and the heat affected zone in 3CR12 welds. a) E309L + pure argon b)E309L + (Ar + 33%N2) c) E307 + pure argon. (GMAW, HI = 1.2kJ/mm, etched by quick swabbing with Kalling's no. 2)

A larger fraction of grain boundary martensite was present in the heat affected zones of the E307 weld (with pure argon) and the E309L weld (with the argon-nitrogen mixture) than in the heat affected zone of the E309L weld (with pure argon shielding gas). Image analysis readings yielded 30% grain boundary martensite in the heat affected zone of the E309L weld (with pure argon), 42.1% grain boundary martensite in the heat affected zone of the E307 weld (with pure argon) and 41% grain boundary martensite in the heat affected zone of the E309L weld (with the argon-nitrogen mixture). The smaller grain size and larger fraction of martensite in the case of E307 and E309L (with Ar-N_2 mixture) suggest that diffusion of interstitial elements across the fusion line into the heat affected zone took place, and that the microstructure of the heat affected zone can be altered to a certain extent by this procedure.

Table 4.7: ASTM grain size numbers in the high temperature heat affected zone (GMAW, 1.2kJ/mm, E309L filler wire, pure argon shielding gas)

Number	L (cm)	n	M	N	N from ASTM eyepiece	Matching grain size (μm)
1	25.1	4	400	1.9	1-2	200-300
2	25.1	4	400	1.9	1-2	200-300
3	25.1	4	400	1.9	1-2	200-300
4	25.1	4	400	1.9	1-2	200-300
Average				1.9		

Table 4.8: ASTM grain size number in the high temperature heat affected zone (GMAW, 1.2kJ/mm, E309L filler wire with Ar + 33% N2 shielding gas)

Number	L (cm)	n	M	N	N from ASTM eyepiece	Matching grain size (μm)
1	25.1	11	400	4.9	4-5	70-80
2	25.1	10	400	4.6	4-5	70-80
3	25.1	11	400	4.9	4-5	70-80
4	25.1	12	400	5.1	4-5	70-80
Average				4.9		

Table 4.9: ASTM grain size numbers in the high temperature heat affected zone (GMAW, 1.2kJ/mm, E307 filler wire, pure argon shielding gas)

Number	L (cm)	n	M	N	N from ASTM eyepiece	Matching grain size (μm)
1	25.1	13	400	5.4	4-5	70-80
2	25.1	14	400	5.6	4-5	70-80
3	25.1	13	400	5.4	4-5	70-80
4	25.1	12	400	5.1	4-5	70-80
Average				5.4		

4.3.4.1 Charpy V-notch testing and results

Six Charpy impact (10mm × 10mm × 55mm) specimens were prepared from each of the welds. A butter layer K-type preparation was used. The V-notch was carefully directed into the heat-affected zone, parallel to the welding direction. In the E309L weld with the argon-nitrogen mixture and in the E307 weld with the pure argon shielding gas, the crack deviated into the parent metal in the central region of the specimen. In the E309L weld with pure argon shielding gas, the heat affected zone failures appeared bright and intergranular with the crack propagating straight through the grain growth zone without deviation. The facet size corresponded with the grain size observed earlier. Hardness profiles across the three welds are shown in figure 4.17 and the Charpy impact energy results are given in figure 4.18. Figure 4.17 indicates that the hardness of the weld metal of the three welds is approximately the same. The HAZ of the E307 welds is much harder than that of the E309L welds. The E307 HAZ is also more impact resistant as a result of the finer grain structure. The HAZ is more likely to be protected by plastic deformation of the 3CR12 parent metal and the E307 weld metal. As a result, the overall impact resistance of a joint in 3CR12 with an E307 filler would be larger than a joint with an E309L filler.

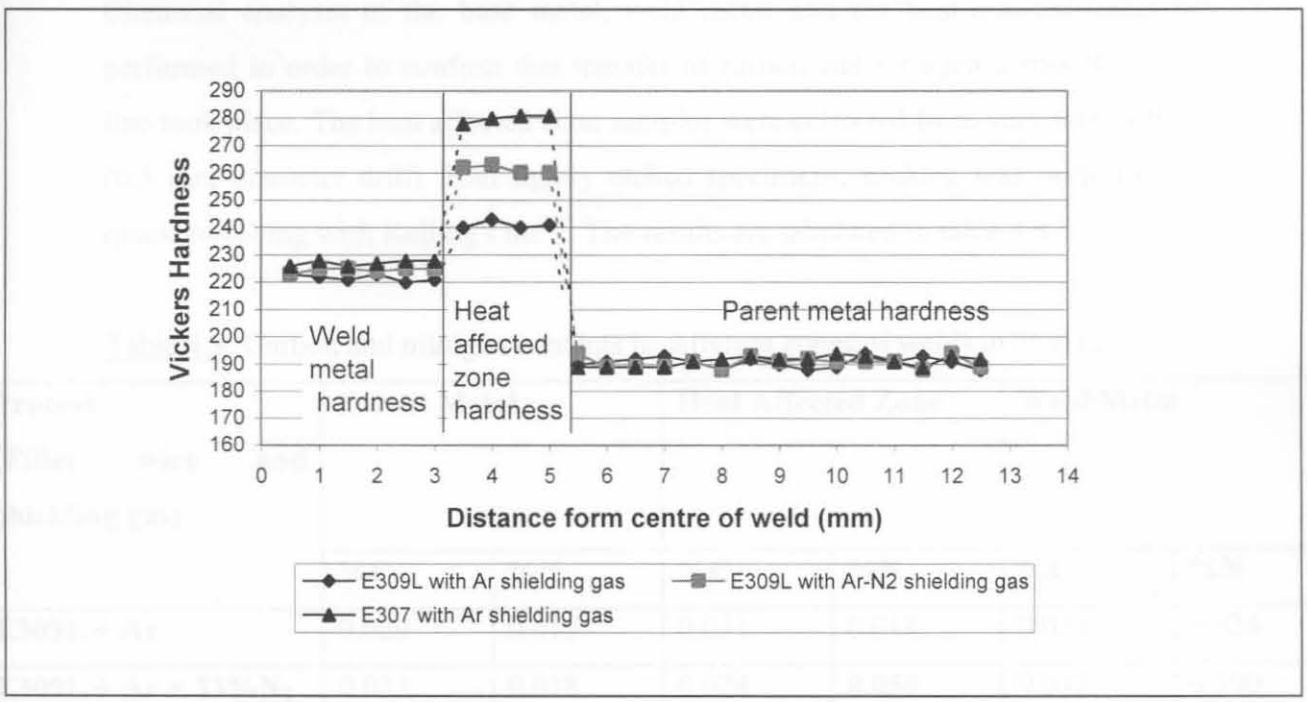

Figure 4.17: Hardness profile for welds in 3CR12 (GMAW, HI = 1.2kJ/mm)

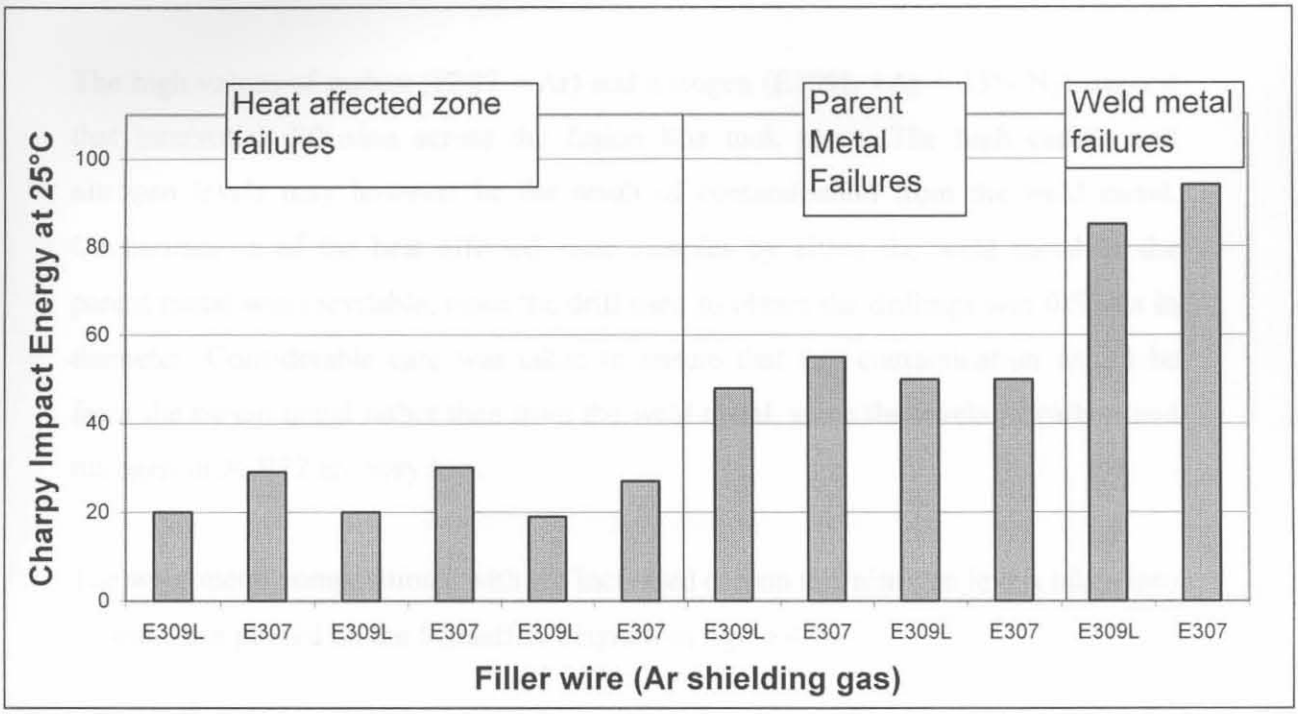

Figure 4.18: Charpy Impact Energy values at 20 C. (GMAW, HI = 1.2kJ/mm)

4.3.4.2 Chemical analysis

Chemical analysis of the base metal, weld metal and the heat-affected zone was performed in order to confirm that transfer of carbon and nitrogen across the fusion line took place. The heat affected zone samples were collected from very fine drillings (0.5 mm diameter drill) from lightly etched specimens. Etching was performed by quick swabbing with Kalling's no. 2. The results are tabulated in table 4.8.

Table 4.8: Carbon and nitrogen contents in different zones of welds in 3CR12.

Process (Filler wire and shielding gas)	**Parent Metal**		**Heat Affected Zone**		**Weld Metal**	
	%C	**%N**	**%C**	**%N**	**%C**	**%N**
E309L + Ar	0.029	0.019	0.031	0.018	0.032	0.024
E309L + Ar + 33%N_2	0.033	0.018	0.028	**0.050**	0.032	0.500
E307 +Ar	0.027	0.017	**0.053**	0.019	0.130	0.020

The high values of carbon (E307 + Ar) and nitrogen (E309L +Ar + 33% N_2) suggest that interstitial diffusion across the fusion line took place. The high carbon and nitrogen levels may however be the result of contamination from the weld metal. Contamination of the heat affected zone samples by either the weld metal or the parent metal was inevitable, since the drill used to obtain the drillings was 0.5 mm in diameter. Considerable care was taken to ensure that any contamination would be from the parent metal rather than from the weld metal, since the levels of carbon and nitrogen in 3CR12 are very low.

The weld metal compositions, with the increased carbon and nitrogen levels taken into account, are plotted on the Schaeffler diagram in figure 4.19.

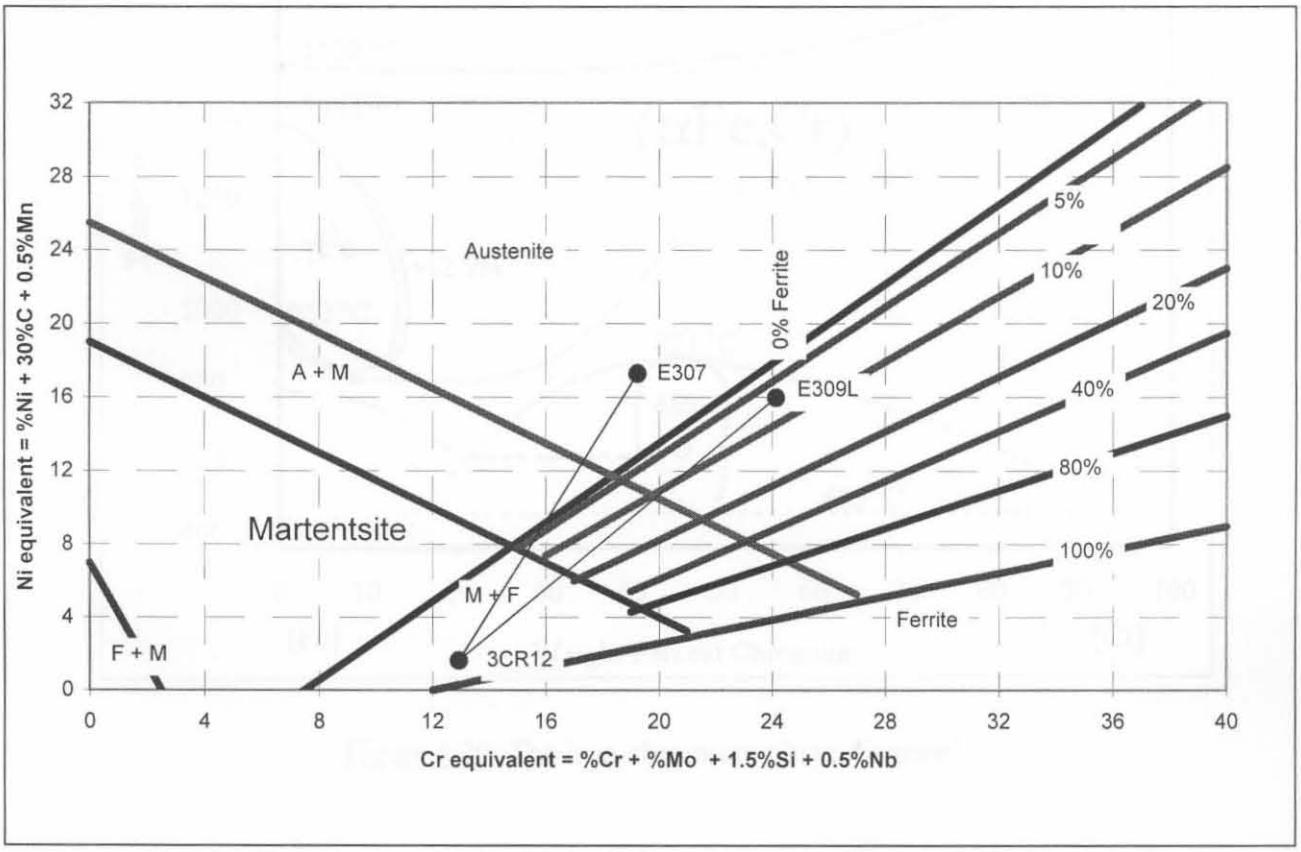

Figure 4.19: The Schaeffler diagram with the two different GMAW experimental welds.

4.4 Post weld heat treatment

4.4.1 Introduction

As discussed earlier, conventional ferritic stainless steels are subject to grain growth in the heat-affected zone, which leads to low toughness levels in thicker plate sections. The grain size cannot be refined as there is an absence of transformation in these steels because their compositions place them on the right side of the gamma loop on the iron-chromium equilibrium diagram (figure 4.20)[1] A similar problem is experienced during the welding of 3CR12, with the difference that the composition of 3CR12 places it in the region where a dual phase ferritic-austenitic structure can exist

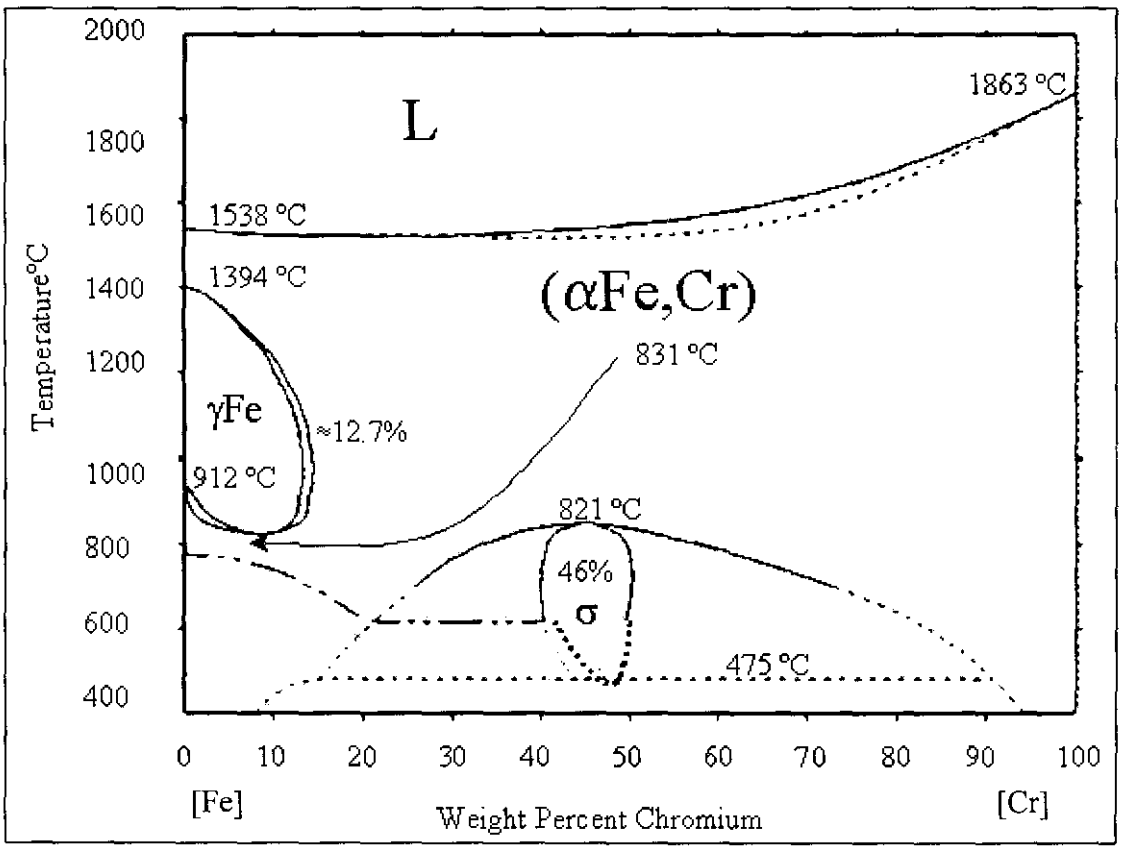

Figure 4.20: The iron-chromium phase diagram[1].

at elevated temperatures, i.e. in the dual phase region on the extreme right of the loop. During welding, the high temperature heat affected zone, as discussed earlier, is heated through the dual phase region into the delta ferrite phase field, and upon cooling some austenite reforms on the grain boundaries. The grain boundary austenite restricts further delta ferrite grain growth during cooling. As the cooling rate through

the dual phase region after welding is rapid, it is unlikely that all the austenite that would have formed in the dual-phase region during slow cooling would form during welding. This suggests that the microstructure of the HAZ can be altered by heat treatment. Especially in view of the influence of martensite as determined by Zaayman[3] (as discussed earlier), the potential importance of post-weld heat treatment was investigated.

4.4.2. Hardening

In simulation experiments carried out by Zaayman[3], a decrease in the DBTT's of two different 11% to 12% chromium steels was detected as soon as the martensite content of these steels exceeded 90% after austenitizing at 1000 °C. This occurred in spite of an increase in hardness. The beneficial effect of the finer structure resulting from the formation of martensite exceeded the detrimental effect of increased hardness[3]. Austenitizing the heat affected zone could result in an improvement in the impact properties of the weld, as the large fraction of austenite that exist in the microstructure at elevated temperatures transform to martensite on cooling. This transformation refines the structure.

Most of the carbon in a ferric-martensitic stainless steel segregate to the austenite in the dual-phase region at elevated temperatures. The austenite is normally air hardenable[10] to a large extent, and it can be assumed that the austenite in the high temperature heat affected zone of 3CR12 will transform to martensite upon air cooling. In order to obtain a fully martensitic structure during air cooling, two conditions[10] have to be met:

1. The balance of alloying elements must produce a fully austenitic structure at the austenitizing temperature, e.g. 1050 °C.
2. The M_s to M_f temperature range must be above room temperature to eliminate retained austenite.

The M_s of the austenite in 3CR12 is well above room temperature, and the M_s to M_f range is expected to be above room temperature. As a result, all the austenite that formed during the austenitizing heat treatment would probably transform to martensite.

4.4.3 Tempering

Based on simulation experiments, Zaayman[3] reported a decrease in DBTT of 70°C and 30°C respectively in two different 11% to 12% chromium steel heats after tempering a 95% and a 100% martensite structure at 750 °C for 1 hour. The beneficial effect of tempering is due to a decrease in hardness of the martensite structure caused by the precipitation and growth of carbides in the martensite matrix. The influence of higher carbon and nitrogen content would be to increase the tempering resistance of the steel, as shown in figure 4.21[1]. The increase in tempering resistance causes the structure to be slightly harder after tempering than a structure with less carbon, but a decrease in hardness still occurs during tempering. The decrease in hardness is sufficient to cause an improvement in the impact properties of the structure. It is expected that tempering would be an appropriate method of improving the fracture toughness of the heat affected zone after hardening. The temper parameter is given by equation (4.5)[1].

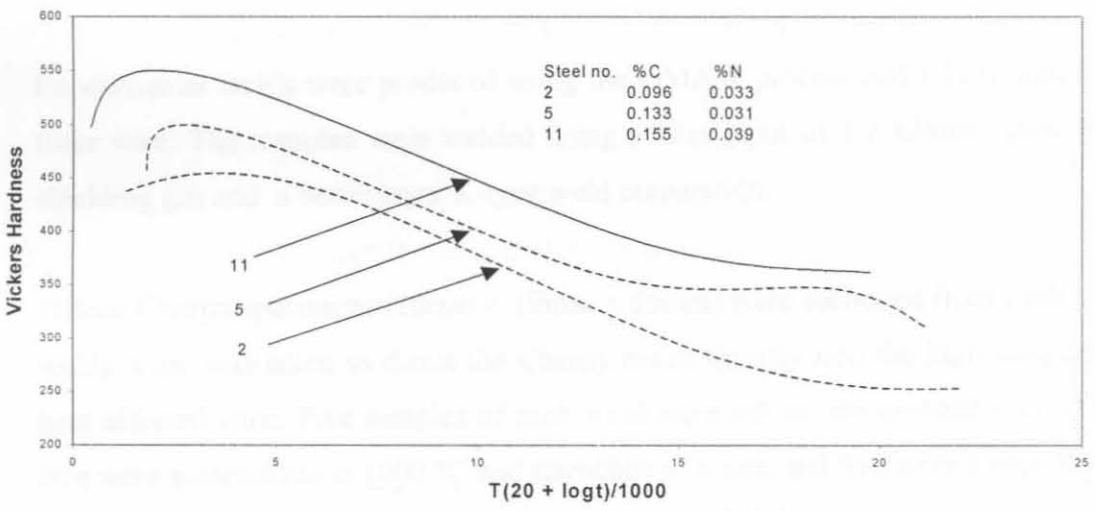

Figure 4.21: The effect of carbon and nitrogen on the tempering of a 12% Cr steel[1].

$$P = T(k + \log t) \quad .....(4.5)$$

where P = temper parameter

T = temperature in K

k = constant = 20 for alloy steels[1]

t = time in hours

Temper curves for stainless steels indicate that a temper parameter of about 21 000 is required to decrease the hardness to a value less than 200 DPN during tempering.[1] That would translate into 1050K (777 °C) for 1 hour. If the increase in tempering resistance is taken into account, a temper heat treatment for 1 hour at approximately 800 °C would be reasonable practice to improve the impact strength of the heat affected zone in 3CR12 after hardening. The proposed tempering heat treatment temperature is high: just below the ferrite-to-austenite transformation temperature at approximately 820 °C.

4.4.4 Experimental heat treatment and results

Experimental welds were produced using the GMAW process and E309L and E307 filler wire. The samples were welded using a heat input of 1.2 kJ/mm, pure argon shielding gas and a butter layer K-type weld preparation.

Fifteen Charpy specimens (10mm × 10mm × 55mm) were sectioned from each of the welds. Care was taken to direct the Charpy notch directly into the high temperature heat affected zone. Five samples of each weld were left in the as-welded condition, five were austenitized at 1000 °C and quenched in water, and five were austenitized at 1000 °C, water quenched and tempered for 1 hour at 800 °C.

Image analysis yielded 35% martensite in the heat affected zone of the as-welded E309L welds. After hardening, 80% martensite was recorded. The hardened and tempered samples yielded 82% martensite in the heat affected zone.

The as-welded E307 samples contained 44% martensite in the heat affected zone, and after hardening 87.5% martensite was recorded. The hardened and tempered samples yielded 86% martensite in the heat affected zone.

From the results of the impact tests as shown in figure 4.22 it is evident that the hardening heat treatment caused an improvement in the impact properties of the heat affected zone. Further improvement through tempering was limited to the E307 welds. Tempering did not markedly improve the impact properties of the heat affected zone in the E309L welds. The driving force for carbide precipitation in the heat affected zone of the E307 welds is greater due to the higher carbon content. For this reason, the first stages of tempering may be faster in the heat affected zone of the E309L welds. Post-weld heat treatment did not alter the impact properties of the parent metal or the weld metal of both welds.

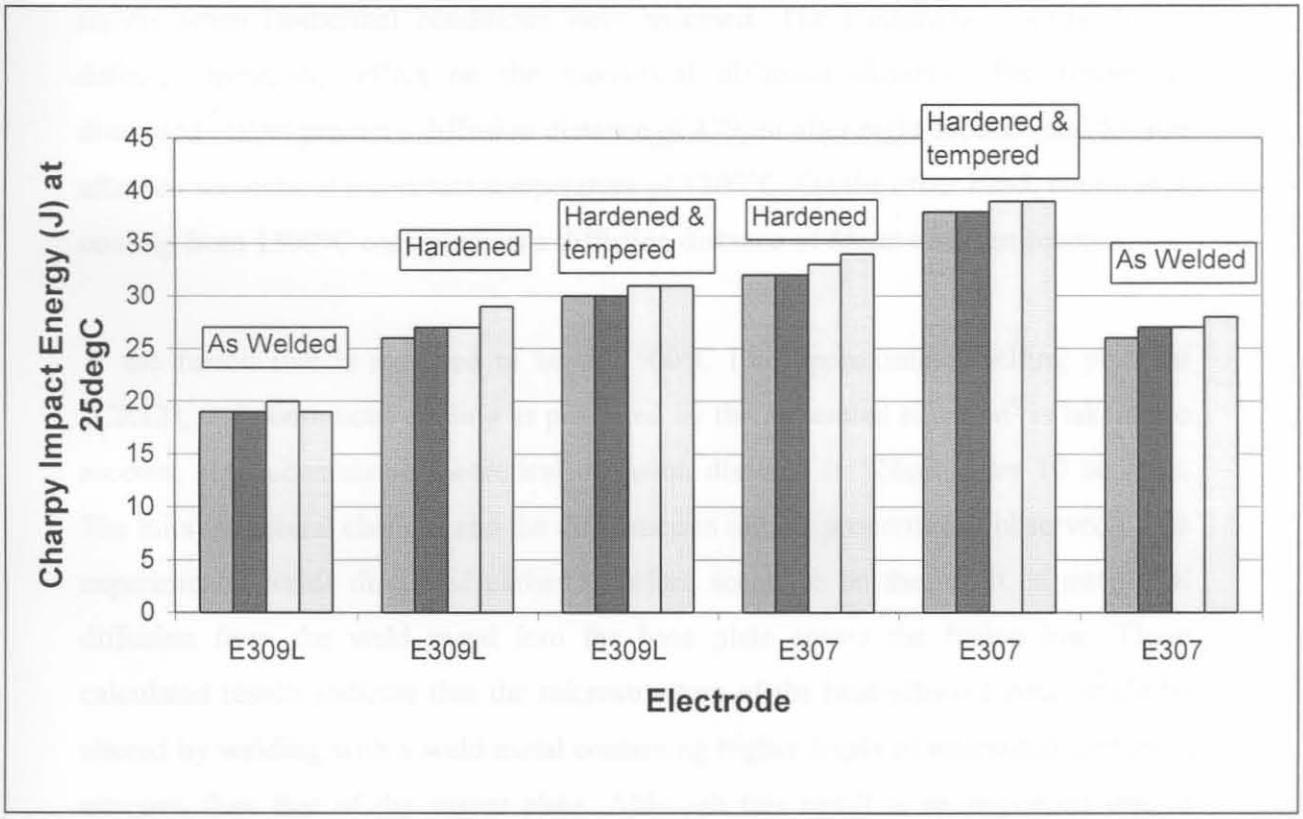

Figure 4.22: Charpy Impact energy values in the heat affected zone at 20 °C.
(GMAW, HI = 1.3 kJ/mm)

4.5 Continuous cooling and diffusion.

It was mentioned earlier that the isothermal conditions assumed in the diffusion distance calculations were not valid, since the welded plate cools continuously. In order to get a more acceptable model of the interstitial diffusion of carbon during the cooling period of a weld, a temperature sequence for the fusion line (1500°C) of a 1.0 kJ/mm weld in 12mm 3CR12 plate was constructed from the Rosenthal equation[1]. In order to construct the sequence, a period of 40 seconds was divided into time intervals of 0.1 seconds. The diffusion coefficient was calculated at the end of each interval, using the temperature at that time. The average diffusion coefficient was then determined after 1 second, 2 seconds et cetera, up to 10 seconds.

The results of these calculations are shown in figure 4.23, together with the earlier results when isothermal conditions were assumed. The continuous cooling has a definite decreasing effect on the theoretical diffusion distance. The results as discussed earlier predict a diffusion distance of 479μm after eight seconds and 535μm after ten seconds, at a constant temperature of 1300°C. On the other hand, continuous cooling from 1300°C only predicts a diffusion distance of 85μm after ten seconds.

If the fusion line is assumed to be at 1500°C (the approximate melting point of 3CR12), and continuous cooling as predicted by the Rosenthal equation[4] is taken into account, the accumulated theoretical diffusion distance is 326μm after 10 seconds. The microstructural changes and the difference in impact properties as observed in the experimental welds discussed earlier therefore seems to be the result of interstitial diffusion from the weld metal into the base plate across the fusion line. These calculated results indicate that the microstructure of the heat-affected zone might be altered by welding with a weld metal containing higher levels of interstitial carbon or nitrogen than that of the parent plate. Although this result is an important one, it should be mentioned that an increase in carbon might give rise to sensitizing and subsequent loss of corrosion resistance of the 3CR12 parent plate. The aim of this study was however to investigate the possibility of changing the heat affected zone microstructure, and sensitizing behaviour was not investigated.

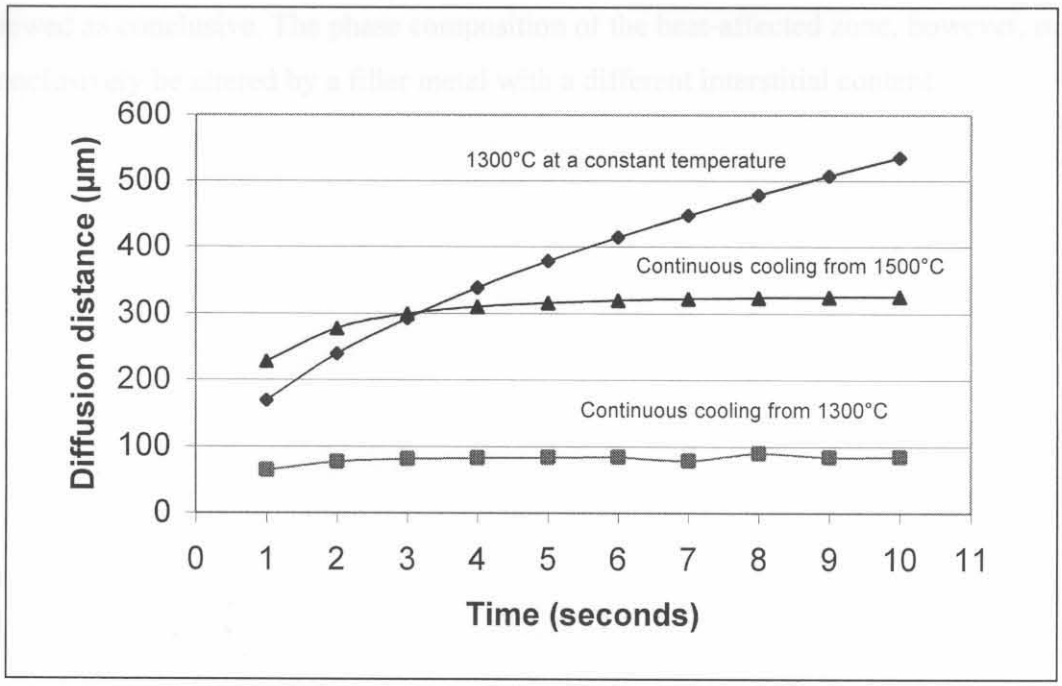

Figure 4.23: Diffusion distance calculated for carbon in 3CR12 for a constant temperature of 1300°C and continuous cooling from 1300°C and 1500°C

4.6 Conclusions

Ferrite grain size in the heat-affected zones of welds in 3CR12 has a detrimental effect on the impact properties of the welded joint. Ferrite grain growth can be inhibited by increasing the high temperature renge where austenite is stable. Increasing carbon or nitrogen contents in the heat-affected zone should also increase grain boundary austenite. Consequently, a decrease in ferrite grain growth should be observed in the heat-affected zone of 3CR12 welds.

A decrease in the ferrite grain size occurs in the heat-affected zones of welds in 3CR12 if the carbon or nitrogen content of the weld metal is increased. The finer heat affected zone structure improves the impact properties of the welded joint. Diffusion distance calculations suggest that the finer structure, increase in grain boundary austenite and improvement in impact properties are the result of diffusion of carbon and nitrogen from the weld metal, across the fusion line and into the heat-affected zone. Although an increase in the interstitial content of the heat-affected zone was observed in chemical analysis, contamination of the heat-affected zone samples by the weld metal could not be ruled out. Therefore, the chemical analysis should not be

viewed as conclusive. The phase composition of the heat-affected zone, however, may conclusively be altered by a filler metal with a different interstitial content.

4.7 References

1. Llewellyn, D.T.; Steels: Metallurgy and applications; Butterwoth-Heimemann Oxford; Second Edition 1994; Second Impression 1995; pp. 221-262.

2. Easterling, K; Introduction to the physical metallurgy of welding; Butterworth-Heinemann Oxford; Second Edition 1992; Second Impression 1993; pp.1-38.

3. Zaayman, J.J.J.; Improvements to the toughness of the heat affected zone in welds of 11 to 12 per cent chromium steels; Ph.D. UP (1994); pp. 23-101.

3. Grobler, C; Weldability studies on 12% and 14% chromium steels; Ph.D. (UP) (1987); pp. 1- 15.

5. Gooch, T.G & Ginn, T.G; Heat affected zone toughness of MMA welded 12%Cr martensitic- ferritic steels; Report from the co-operative research programme for research members only; The welding institute; Cambridge 1988; pp.1-9.

6. Product Guide for 3CR12; Middelburg Steel and Alloys (Pty) Limited; January 1988; pp. 14-19

7. Stumpf, W.E; Fasetransformasies in die vaste toestand; Kursus op die nagraadse vlak (UP); Uitgawe vir 1995; pp. 307-309.

8. Weertman J. & Weertman J.R.; Elementary Dislocation Theory; The Macmillan Company New York 1964; pp. 1-15

9. Hawkins, D.N, Beech, J & Valtierra-Gallardo, S; A new approach to microstructural control in duplex stainless steel welds; Sheffield; 1988; pp. 199-203.

10. Thelning, K.E; Steel and its heat treatment; Butterworths London; Second Edition 1988; pp. 24-30.

11. Bakker, H et al; Landolt-Börnstein Zahlenwerte und Funktionen aus Naturwissenschaftenund Technik; Herausgeber H. Meherer; Band 26; Springer-Verlag Berlin; pp. 481.

12. Kotecki, D.J; (Technical director for stainless and high alloy product development, Lincoln Electric Company Cleveland, Ohio USA); Welding stainless steels; Lecture at the South African Institute of Welding; September 1996.

13. Product Guide for 3CR12; Middelburg Steel and Alloys (Pty) Limited; January 1988; pp. 14-19

14. Holman, J.P.; Heat Transfer; McGraw-Hill Book Company New York 1989; pp. 633-650.